JOURNAL OF SOLID STATE CHEMISTRY 112, 126–131 (1994)

Structure Refinement of the 0201–1201 Intergrowth-Type Ferrite $PbSr_4Fe_2O_9$: Powder Neutron Diffraction and Mössbauer Spectroscopy Studies

V. Caignaert, Ph. Daniel, N. Nguyen, A. Ducouret, D. Groult, and B. Raveau

Laboratoire CRISMAT (CNRS, URA 1318) ISMRA, Université de Caen, 6 boulevard du Maréchal Juin, 14050 Caen Cédex, France

Received January 3, 1994; in revised form May 2, 1994; accepted May 4, 1994

The structure of the tetragonal ferrite $PbSr_4Fe_2O_9$ (a = 3.8484 Å, c = 30.683 Å) has been refined from powder neutron diffraction data. The intergrowth of the two structures 0201 and 1201 with the La_2CuO_4 and the $TlSr_2CuO_5$ types is confirmed as is the oxygen stoichiometry (O_9), which involve oxidation states III and IV for iron and lead, respectively. The structure of the $[PbO]_\infty$ layers consists of two sets of Pb sites (at the origin and on 8*i* (x00) split positions) and one set of oxygen atoms O(1) on 8*j* (x½0) split positions. According to neutron diffraction, Mössbauer spectroscopy, and electric field gradient calculations, a splitting of the axial oxygen [O(2)] along the c direction appears also as most probable. It results in two highly distorted octahedral coordinations for Fe(III), which can be better described as almost regular $[FeO_5]$ pyramids. Similarly two coordination states are found for Pb(IV): a flattened $[PbO_6]$ octahedron and a distorted $[PbO_4]$ tetrahedron.

INTRODUCTION

Substitution of iron for copper in high T_c superconducting layered cuprates is of critical importance for understanding the relationships between structure, chemical bonding, and superconductivity in these materials. For this reason, iron has been extensively used as a local probe to study the magnetic behavior of the 92 K superconductor $YBa_2Cu_3O_7$ (1–8). New series of ferrites closely related to the layered cuprates and corresponding to different intergrowths 0201 (9), 2201 (10), 1212 (11), 2212 (12, 13), and 2223 (14) recently have been isolated. Among them, the lead-based iron oxides (11, 15) are of great interest owing to the possible coexistence of the redox couples Pb(IV)/Pb(II) and Fe(III)Fe(IV) that make it difficult to understand oxygen nonstoichiometry in these compounds. Moreover, besides knowledge of iron coordination, which can be pyramidal, octahedral, or even tetrahedral in these phases, a second issue, that of the structure of the intermediate lead-oxygen layers, must be resolved. A structural investigation of these layers should help clarify the behavior of lead in high T_c cuprates which indeed exhibit a high degree of atomic disorder at the level of the mixed $[(Pb_{1-x}A_x)O]_\infty$ rock salt-type layers (A = Cu, Cd, Ca, Sr, Hg, Mg, V) (16–22).

In this respect the recently isolated (15) tetragonal ferrite $PbSr_4Fe_2O_9$ is an interesting candidate owing to the simplicity of its formulation, implying the existence of fully occupied single $[PbO]_\infty$ layers. The preliminary powder X-ray investigation indeed suggested that the phase consists of stacked $[PbO]_\infty$, $[SrO]_\infty$ layers with single perovskite layers $[SrFeO_3]_\infty$, so that the ideal structure (Fig. 1) should be described as an intergrowth of 0201 and 1201 structures corresponding to slices with compositions Sr_2FeO_4 and $PbSr_2FeO_5$, respectively. We report here on the powder neutron diffraction analysis and Mössbauer spectroscopy study of $PbSr_4Fe_2O_9$, coupled to EFG calculations.

EXPERIMENTAL

Samples of $PbSr_4Fe_2O_9$ have been prepared from mixtures of the starting materials PbO, $SrCO_3$, and Fe_2O_3 as described elsewhere (15).

Neutron powder diffraction measurements were made at room temperature with the high resolution diffractometer $3T_2$ at LLB (Saclay) using a wavelength of 1.2269 Å. Intensities were measured between 5° and 120° (2θ) with increments of 0.05°. The structure was refined with the Rietveld method by means of the DBW-3.2 program (23).

The room-temperature Mössbauer spectrum of $PbSr_4Fe_2O_9$ has been recorded by means of a constant-acceleration spectrometer with a $^{57}Co/Rh$ source.

RESULTS AND DISCUSSION

In the idealized model (Fig. 1), which corresponds to the atoms located in the high-symmetry positions of the space group I_4/mmm, the first neutron refinements show that the thermal parameters of the Pb and O atoms forming the [PbO] layers are abnormally high (4.6 and 11.8 Å^2,

0022-4596/94 $6.00

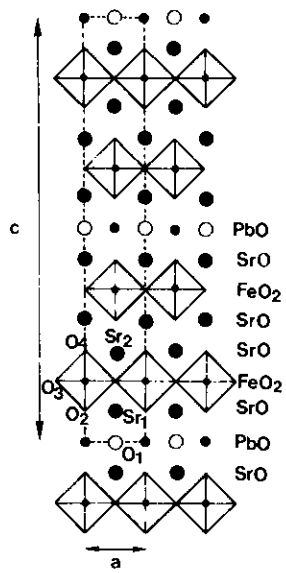

FIG. 1. Schematic drawing of the structure of $PbSr_4Fe_2O_9$.

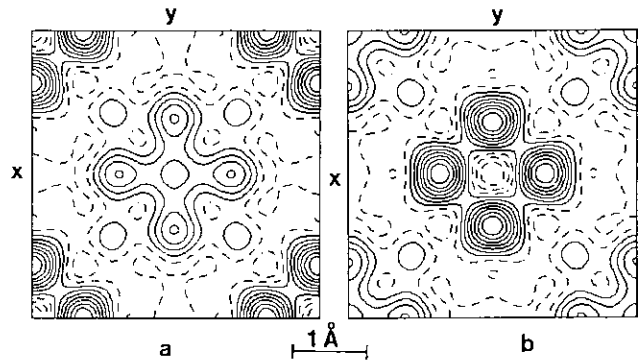

FIG. 2. Fourier sections determined at $z = \frac{1}{2}$ for lead (a) and $z = 0$ for O(1) (b) showing that lead and oxygen atoms of $[PbO]_\infty$ layers must be distributed on split positions.

respectively). Fourier sections performed at the levels of the $[PbO]_\infty$ planes, i.e., $z = 0$ and $z = \frac{1}{2}$ (Fig. 2) show without ambiguity that the oxygen atoms [O(1)] in 2*b* site ($\frac{1}{2}\frac{1}{2}0$) must be split over the eight positions 8*j* ($x\frac{1}{2}0$). In the same way a splitting of the Pb atoms between the eight positions 8*i* ($x00$) must be considered. However, it should be pointed out that the Fourier map corresponding to the lead atoms suggests a partial occupancy of both sites 2*a* (000) and 8*i* ($x00$). Therefore, subsequent refinements were then performed with O(1) atoms in 8*j* ($x\frac{1}{2}0$) and Pb atoms on 2*a* (000) and 8*i* ($x00$) simultaneously. This significantly improves the discrepancy factor and results in acceptable values of the thermal parameters for Pb and O(1). At this stage of the refinement, one observes that the isotropic thermal factor of the oxygen O(2) which corresponds to the apical Pb–O bond (parallel to **c**) remains rather high (close to 3 Å^2).

The refinement of the anisotropic thermal parameters of this atom clearly establishes that there exists a larger displacement along **c** ($U_{11} = U_{22} = 0.0348$ Å^2, $U_{33} = 0.0501$ Å^2) which might correspond to a splitting of the [O(2)] site into two other atoms. Although it has not been clearly evidenced from X-ray or neutron diffraction structural characterizations (24, 25), the existence of two equally populated axial oxygen sites separated by 0.10–0.15 Å was first suggested in $YBa_2Cu_3O_7$ and Tl-based superconductors from Cu*K* edge-polarized EXAFS data (26, 27) and ion-channeling experiments (28).

The final results of our calculations are given in Table 1 and a plot of the calculated and observed profiles is shown in Fig. 3 corresponding to the conventional Riet-

TABLE 1
Refined Structural Parameters of $PbSr_4Fe_2O_9$ at Room Temperature[a]

Atom	Position	*x*	*y*	*z*	*B* (Å)^2	Occupancy
Pb(1) 2*a*	4/*mmm*	0	0	0	2.1(2)	0.62(3)
Pb(2) 8*i*	*mm*	0.140(8)	0	0	2.1(2)	0.39(3)
Sr(1) 4*e*	4*mm*	0.5	0.5	0.0855(1)	0.74(5)	2
Sr(2) 4*e*	4*mm*	0.5	0.5	0.2050(1)	0.54(4)	2
Fe 4*e*	4*mm*	0	0	0.1512(1)	0.35(3)	2
O(1) 8*j*	*mm*	0.141(2)	0	0.5	1.8(2)	1
O(2) 4*e*	4*mm*	0	0	0.0642(1)	3.1(2)[b]	2
O(3) 8*g*	*mm*	0.5	0	0.1419(1)	0.60(3)	4
O(4) 4*e*	4*mm*	0	0	0.2145(1)	0.79(5)	2

Note. e.s.d.'s are in parentheses.

[a] Space group I4/*mmm*, $Z = 2$, MW = 813.36 g, $\rho_c = 5.94$ g/cm^3, $a = 3.84845(8)$ Å, $c = 30.6838(8)$ Å, $V = 454.44(3)$ Å^3, $R_p = 15.6\%$, $R_{wp} = 14.1\%$, $R_{exp} = 6.08\%$, $\chi^2 = 5.37$, $R_I = 7.21\%$.

[b] Anisotropic thermal parameters: $U_{11} = U_{22} = 0.0348$ Å^2, $U_{33} = 0.0501$ Å^2, $B_{eq} = 8\pi^2 U_{eq}$.

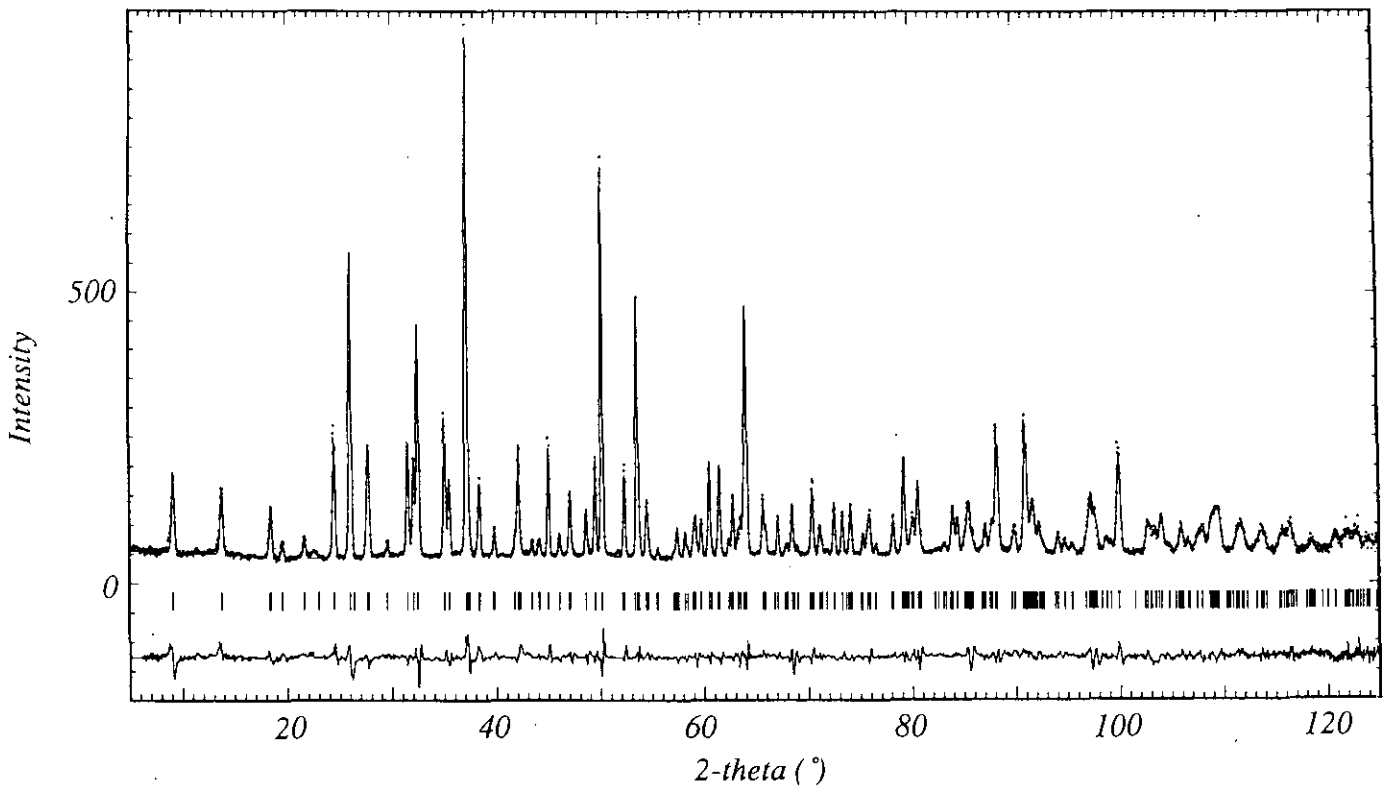

FIG. 3. Observed (small circles) and calculated (continuous line) intensities for the structure of $PbSr_4Fe_2O_9$. The differences ($I_{calc} - I_{obs}$) are shown at the bottom of each plot.

veld factors $R_p = 15.6\%$, $R_{wp} = 14.1\%$, $R_{exp} = 6.08\%$, $\chi^2 = 5.37$ and the Bragg factor $R_I = 7.21\%$.

Note that the identical values of the discrepancy factors can be obtained by locating lead atoms at the origin with a total occupancy and by refining the anisotropic thermal parameters of this element. One obtains abnormally high thermal displacement parameters along *a* and *b* directions ($U_{11} = U_{22} = 0.0709$ Å^2, $U_{33} = 0.0277$ Å^2) which confirm that a distribution of lead over the two sites 2*a* (000) and 8*i* (*x*00) is the most reasonable. Moreover, it is worth pointing out that the cell occupancies of the sites which indicate a preference for the 2*a* site appear in good agreement with previous results reported for lead-based 1212-cuprates. It has indeed been demonstrated from single-crystal X-ray diffraction and powder neutron diffraction data (16–22) of $(Pb_{1-x}A_x)Sr_2(Y_{1-y}Ca_y)Cu_2O_7$ compounds that lead was located at the origin with an occupancy factor ranging from 0.70 to 0.56, in good accordance with the EDS analysis of the samples. Selected interatomic distances have been listed in Table 2.

The Mössbauer spectrum of $PbSr_4Fe_2O_9$ registered at room temperature (Fig. 4) confirms the only presence of Fe(III) in agreement with the oxygen stoichiometry. However, it reveals that two iron sites labeled I and II are needed to correctly fit the experimental asymmetric doublet with the relative intensities 29 and 71%, respectively (Table 3). They correspond to isomer shifts of 0.27 and 0.21 mm/sec, which are typical of high-spin Fe(III) species.

In order to understand the relationships between these two Mössbauer sites and that deduced from neutron diffraction refinements, we have performed electric field gra-

TABLE 2
Selected Interatomic Bond Distances (Å) for $PbSr_4Fe_2O_9$

Pb(1)–O(1) × 4	2.368(5)
–O(2) × 2	1.972(6)
Pb(2)–O(1) × 2	2.10(1)
Pb(2)–O(2) × 2	2.04(1)
Sr(1)–O(1) × 1	2.677(3)
–O(2) × 4	2.798(2)
–O(3) × 4	2.589(3)
Sr(2)–O(3) × 4	2.729(3)
–O(4) × 4	2.737(1)
–O(4) × 1	2.470(4)
Fe–O(2) × 1	2.669(7)
–O(3) × 4	1.946(1)
–O(4) × 1	1.940(4)

Note. e.s.d.'s are in parentheses.

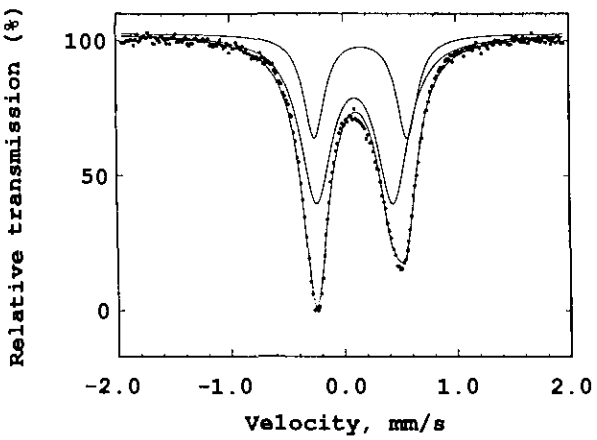

FIG. 4. Mössbauer spectrum of $PbSr_4Fe_2O_9$ registered at room temperature.

dient (EFG) calculations, considering various oxygen environments for high-spin Fe(III).

The quadrupole splitting for Fe(III) results only in the "lattice term" deduced from the main components V_{XX}, V_{YY}, V_{ZZ} of the lattice iron EFG tensor, according to the relation

$$QS = (1 - \gamma_\infty)\frac{eQ}{2}V_{ZZ}\left(1 + \frac{\eta^2}{3}\right)^{1/2},$$

where $(1 - \gamma_\infty)$ is the Sternheimer antishielding factor, Q the quadrupole moment in the excited state $I = \frac{3}{2}$ of the ^{57}Fe nucleus, and η is the asymmetry parameter defined as

$$\eta = (V_{XX} - V_{YY})/V_{ZZ} \quad \text{with} \mid V_{XX} \mid \leq \mid V_{YY} \mid \leq \mid V_{ZZ} \mid .$$

For Fe(III), $(1 - \gamma_\infty)$ has been taken equal to 10.14 (29) and a mean value of 0.2 barn has been chosen for Q, which is found in the literature as varying from 0.08 to 0.28 barn (30, 31).

Lattice EFG calculations have then been computed by taking into account either the whole crystal or the first oxygen neighbors:

—For the whole crystal, the monopolar lattice contribution has been estimated equivalently using either the LATSUM point charge program or the monopolar part of the EFGDIR program (32). Using the atomic positions determined by neutron diffraction, only one monopolar value is obtained for the two Fe sites $\overline{QS}_{cryst} = 0.81$ mm/sec with a V_{ZZ} component which is positive and aligned along **c**. This value is in qualitative agreement with the weighted mean value $\overline{QS}_{MB} = 0.72$ mm/sec corresponding to the Mössbauer quadrupolar splittings 0.68 and 0.82 mm/sec owing to their relative intensities 71 and 29%, respectively.

Note that the difference $\overline{QS}_{MB} - \overline{QS}_{cryst} = -0.09$ mm/sec gives an order of magnitude of the multipolar contribution of the whole crystal to the quadrupole splitting.

—For the contribution of the first oxygen neighbors only, a monopolar program GCE, recently written by one of us (33), has been used allowing the influence of vacancies or atom displacements to be studied.

(i) First, using the refined structural parameters and coordinates of iron and oxygen atoms, listed in Table 1, we obtained a positive V_{ZZ} main component of the EFG tensor, parallel to the **c** axis, in agreement with the results in the whole crystal. It corresponds to a monopolar value $\overline{QS}_{GCE} = 0.77$ mm/sec, relative to a distorted octahedral oxygen environment of the iron ions. The difference $\overline{QS}_{cryst} - \overline{QS}_{GCE} = 0.04$ mm/sec, is representative of the monopolar contribution to QS of the non-nearest neighbors of iron. It has been added to the multipolar contribution of all the iron neighbors to get a total correction of −0.05 mm/sec, which has subsequently been applied to all the GCE-computed QS values before being compared to the experimental Mössbauer ones.

(ii) Second, based on the neutron diffraction data discussed above, which show that the axial oxygen O_2 exhibits anisotropic thermal displacements along **c**, various octahedral oxygen environment of Fe(III) were considered by changing the positional $z(O_2)$ parameter between $z(O_2) = 0.055$ and $z(O_2) = 0.075$.

The results of these calculations have been plotted in Fig. 5. One observes a monotoneous decrease of QS as the positional zO_2 parameter increases. Taking into account the experimental Mössbauer values $QS_I = 0.82$ mm/sec and $QS_{II} = 0.68$ mm/sec for the two observed sites, one obtains the corresponding zO_2 values: $(zO_2)_I = 0.0596(3)$ and $(zO_2)_{II} = 0.0664(3)$.

These values are quite compatible with the mean $zO(2)$ value of 0.0643 deduced from the neutron diffraction study, if one takes into consideration the apparent thermal agitation of the oxygen O(2). As a consequence, although it cannot be clearly proved, the splitting of the oxygen O(2) on two sites along **c** appears most probable, leading to two different octahedral oxygen environments for iron (Table 4).

Note that the absence of oxygen vacancies has been carefully verified by considering successively for iron a

TABLE 3
Mössbauer Resonance Parameters at Room Temperature for $PbSr_4Fe_2O_9$[a]

Site	IS (±0.02) (mm/sec)	Γ (±0.02) (mm/sec)	QS (±0.02) (mm/sec)	Intensity (±5) (%)
I	0.27	0.22	0.82	29
II	0.21	0.34	0.68	71

[a] IS, isomer shift relative to α-Fe; Γ, half-height width; QS, quadrupole splitting; %, fitted intensity of the site.

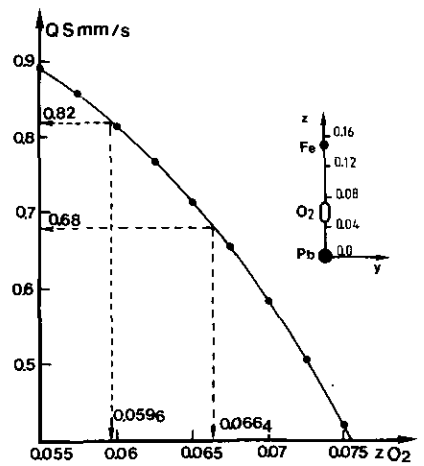

FIG. 5. Quadrupole splittings QS (mm/sec) calculated from monopolar lattice EFGs for high-spin Fe(III) in a distorted octahedral oxygen environment versus the zO(2) positions of the axial oxygens O(2).

pyramidal coordination due to vacancies on either O(2) sites or O(4) sites and even a tetrahedral coordination due to vacancies on the O(3) sites. Lattice EFG calculations indeed lead to QS values of 1.37, 2.45, and 2.87 mm/sec, respectively, much higher than the two experimental values. Therefore the assumption of oxygen vacancies, especially on the O(2) sites must be discarded despite the fact that the Bragg factor can be lowered to $R_I = 5.76\%$ by refining the occupancy rate of O(2) to a value close to 1.79 ± 0.03. Moreover the results of lattice EFGs are in good agreement with the microthermogravimetric analysis experiments, which do not allow any oxygen uptake to be detected after heating of $PbSr_4Fe_2O_9$ samples to 800°C in an oxygen flow.

The Mössbauer and EFG studies explain the existence of two kinds of sites for Pb(IV) species evidenced by neutron diffraction data. When lead is located at the origin, the oxygens O(2) can be displaced along **c** toward the iron atoms (zO(2) ≈ 0.0664) whereas they come closer to the lead atoms (zO(2) ≈ 0.0596) when the Pb(IV) species are distributed over the split 8*i* positions ($x00$), involving acceptable Pb–O distances. This viewpoint is strongly supported by the occupancy factors of the iron and lead sites as shown from the Mössbauer spectroscopy and the neutron diffraction data, respectively.

TABLE 4
Calculated zO(2) Positions Deduced from Lattice EFG Calculations and Corresponding Fe–O(2) Distances (Å)

Mössbauer site	QS (mm/sec)	Calculated zO(2)	Fe–O(2) (Å)	Pb–O(2) (Å)
I	0.82	0.0596(3)	2.81	1.91[a]
II	0.68	0.0664(3)	2.61	2.04[a]

[a] Accounting for the relative intensities of Mössbauer sites I and II (29 and 71%, respectively). Pb–O(2) = 1.91 Å has been obtained by assuming that Pb(IV) was located in $x00$ (Table 1) while Pb–O(2) = 2.04 Å has been calculated for Pb(IV) located at the origin.

This structural study confirms the oxygen stoichiometry of the ferrite $PbSr_4Fe_2O_9$ characterized by the association of Pb(IV) and Fe(III) species. Compared to the isostructural superconducting cuprates $TlBa_{1.6}La_{2.4}Cu_2O_{9-\delta}$ (34) and $HgBa_2La_2Cu_2O_{8-\delta}$ (35), the original features of this phase deal with the local short-range orderings of the oxygen and lead atoms which take place in the $[PbO]_\infty$ layers and with the particular coordination states of lead and iron as shown from the interatomic bond distances listed in Table 2.

Iron is characterized here by its strong tendency to exhibit a pyramidal coordination state. The distorted (FeO_6) octahedra indeed show five almost equal Fe–O distances of 1.94 Å forming an almost regular (FeO_5) pyramid. The sixth apical oxygen O(2) that corresponds to a mean Fe–O bond length of 2.67 Å (or to the distances 2.61 and 2.81 Å according to the Mössbauer study and lattice EFG calculations) is obviously weakly bonded to iron. This dissymmetry can be explained by the presence of Pb(IV), which forms strong covalent apical bonds with O(2). The Pb–O(2) distances are indeed very short, ranging from 2.04 to 1.91 Å if one takes into account the Mössbauer and EFG data or showing a mean value of 2.00 Å if one considers the powder neutron diffraction data.

The distribution of the oxygen atoms over split positions in the $[PbO]_\infty$ planes implies two kinds of coordinations for Pb(IV). The first, which corresponds to Pb in the 2*a* sites, can be described as a flattened (PbO_6) octahedron with two very short apical Pb–O distances (1.97 Å) and four equatorial long distances (2.37 Å). The second, corresponding to Pb in split sites 8*i* ($x00$) can be considered as a distorted (PbO_4) tetrahedron with two apical Pb–O bond lengths of 2.04 Å and two equatorial bond lengths of 2.10 Å. Such (PbO_4) tetrahedra forming chains along the ⟨100⟩ directions of the tetragonal unit cell can be expected only on a local scale since they should form domains with an orthorhombic symmetry as previously suggested for thallium-based superconductors (36). It should be pointed out that such a tetrahedral coordination for Pb(IV) is quite unusual and has not yet been observed to our knowledge. Nevertheless, its $5d^{10}$ electronic configuration, similar to that of Tl(III), which exhibits a tetrahedral coordination in several oxides such as $Tl_2Ba_2O_5$ or $TlLi_5O_4$ (37, 38), supports this model.

In summary, this structure refinement of the lead ferrite $PbSr_4Fe_2O_9$ from powder neutron diffraction data and Mössbauer spectroscopy confirms the validity of the structural model described previously from high-resolution electron microscopy and powder XRD investigations (15) but appears in complete disagreement with the 2212 structure reported recently by T. Fries *et al.* (39).

Further, the great similarity between Tl(III) and Pb(IV) species leads us to think that similar thallium ferrites should be synthesized. Exploration of the systems Tl–Sr–Fe–O and Tl–Pb–Sr–Fe–O, which involve mixed oxidation states for iron, i.e., Fe(IV)/Fe(III), is thus in progress in order to understand the structural behavior of the $[TlO]_\infty$ and $[PbO]_\infty$ layers in these compounds.

REFERENCES

1. G. Xiao, F. H. Streitz, A. Gavrin, Y. W. Du, and C. L. Chien, *Phys. Rev. B* **35,** 8722 (1987).
2. J. M. Tarascon, P. Barboux, P. F. Micelli, L. H. Greene, G. W. Hull, M. Eibschutz, and S. A. Sunshine, *Phys. Rev. B* **37,** (1988).
3. P. Bordet, J. L. Hodeau, P. Strobel, M. Marezio, A. Santoro, C. Chaillout, and J. J. Capponni, *Physica C* **153–155,** 582 (1988).
4. M. Hennion, I. Mirebeau, G. Goddens, A. Menelle, T. E. Phillips, K. Moorjani, and M. Hervieu, *Physica C* **159,** 124 (1989).
5. E. Suard, V. Caignaert, A. Maignan, and B. Raveau, *Physica C* **182,** 219 (1991).
6. Q. Huang, P. Karen, V. L. Karen, A. Kjekshus, J. W. Lynn, A. D. Mighell, N. Rosov, and A. Santoro, *Phys. Rev. B* **45,** 9611 (1992).
7. A. Rykov, V. Caignaert, N. Nguyen, A. Maignan, E. Suard, and B. Raveau, *Physica C* **205,** 63 (1993).
8. E. Garcia-Gonzalez, M. Parras, J. M. Gonzalez-Calbet, and M. Vallet-Regi, *J. Solid State Chem.* **104,** 232 (1993).
9. S. E. Dann, M. T. Weller, and D. B. Currie, *J. Solid State Chem.* **92,** 237 (1991).
10. J. M. Tarascon, Y. Le Page, W. R. Mc. Kinnon, R. Ramesh, M. Eibschutz, E. Tselepis, E. Wang, and G. W. Hull, *Physica C* **167,** 20 (1990).
11. Ph. Daniel, L. Barbey, N. Nguyen, A. Ducouret, D. Groult, and B. Raveau, submitted for publication.
12. M. Hervieu, C. Michel, N. Nguyen, R. Retoux, and B. Raveau, *Eur. J. Solid State Inorg. Chem.* **25,** 375 (1988).
13. Y. Le Page, W. R. Mc. Kinnon, J. M. Tarascon, and P. Barboux, *Phys. Rev. B* **40,** 6810 (1989).
14. R. Retoux, C. Michel, M. Hervieu, N. Nguyen, and B. Raveau, *Solid State Commun.* **69,** 599 (1989).
15. S. Lucas, D. Groult, N. Nguyen, C. Michel, M. Hervieu, and B. Raveau, *J. Solid State Chem.* **102,** 20 (1993).
16. M. A. Subramanian, J. Gopalakrishnan, C. C. Torrardi, D. L. Gai, E. D. Boyes, T. R. Askew, R. B. Flipper, N. E. Farneth, and A. W. Sleight, *Physica C* **157,** 124 (1989).
17. J. Y. Lee, J. S. Swinnea, and H. Steinfink, *J. Mater. Res.* **4,** 763 (1989).
18. T. Maeda, K. Sakuyama, F. Izumi, H. Yamauchi, H. Asuno, and S. Tanaka, *Physica C,* **175** 393 (1991).
19. M. Ledesert, Ph. Labbé, D. Groult, Ph. Daniel, M. Hervieu, and B. Raveau, *Eur. J. Solid State Inorg. Chem.* **30,** 357 (1993).
20. S. F. Hu, D. A. Jefferson, R. S. Liu, and P. P. Edwards, *J. Solid State Chem.* **103,** 280 (1993).
21. W. Widder, M. Franz, L. Bauernfeind, and H. F. Braun, *Physica C* **217,** 121 (1993).
22. T. Rouillon, Thesis, University of Caen, 1992.
23. D. B. Wiles and R. A. Young, *J. Appl. Crystallogr.* **14,** 149 (1981).
24. J. D. Jorgensen, B. W. Veal, A. P. Paulikas, L. J. Nowicki, G. W. Crabtree, H. Claus, and W. K. Kwok, *Phys. Rev. B* **41,** 1863 (1990).
25. J. D. Sullivan, P. Bordet, M. Marezio, K. Takenada, and S. Uchida, *Phys. Rev. B* **48,** 10638 (1993).
26. J. Mustre de Leon, S. D. Conradson, I. Batistic, and A. R. Bishop, *Phys. Rev. Lett.* **65,** 1675 (1990).
27. P. G. Allen, J. Mustre de Leon, S. D. Conradson, and A. R. Bishop, *Phys. Rev. B* **44,** 9480 (1991).
28. R. P. Sharma, L. E. Rehn, P. M. Baldo, and J. Z. Liu, *Phys. Rev. Lett.* **62,** 2869 (1989).
29. R. M. Sternheimer, *Phys. Rev.* **130,** 1423 (1963).
30. P. Gütlich, R. Link, and A. Trautwein, *in* "Mössbauer Spectroscopy and Transition Metal Chemistry," (Inorganic Chemistry Concepts, Vol. 3) (M. Becke, M. F. Lappert, J. L. Margrave, R. W. Parry, C. K. Jorgensen, S. J. Lippard, K. Niedenzu, and H. Yamatera, Eds.). Springer Verlag, Berlin, 1978.
31. K. J. Duff, K. C. Mishra, and T. P. Das, *Phys. Rev. Lett.* **46,** 1611 (1981).
32. Y. Calage, J. Teillet, and F. Varret, "EFGDIR Program," 1982; J. Pannetier, Monopolar LATSUM program using Bertaut's series, 1978, completed by Y. Calage, 1983, unpublished programs.
33. A. Ducouret-Cérèze, Monopolar GCE program, unpublished, 1992.
34. C. Martin, A. Maignan, M. Huvé, M. Hervieu, C. Michel, and B. Raveau, *Physica C* **179,** 1 (1991).
35. M. Huvé, C. Martin, G. Van Tendeloo, A. Maignan, C. Michel, M. Hervieu and B. Raveau *Solid State Commun.* **90,** 37, (1994).
36. W. Dmowski, B. H. Toby, T. Egami, M. A. Subramanian, J. Gopalakrishnan, and A. W. Sleight, *Phys. Rev. Lett.* **61,** 2608 (1988).
37. R. V. Schenck and H. Müller-Buschbaum, *Z. Anorg. Allg. Chem.* **405,** 197 (1974).
38. R. Hoppe and P. Panek, *Z. Anorg. Allg. Chem.* **381,** 129 (1971).
39. T. Fries, C. Steudtner, M. Schlichenmaier, S. Kemmler-Sack, T. Nissel, and R. P. Huebener, *J. Solid State Chem* **109,** 88 (1994).